MATHEMATICAL MODEL FOR LITTORAL DRIFT

By Rolf Deigaard,[1] Jørgen Fredsøe,[2] and Ida Brøker Hedegaard[3]

ABSTRACT: The longshore sediment transport along the coast is investigated by use of detailed sediment transport models in the surf zone. Combined with a detailed description of the wave height and longshore current distribution in the surf-zone, the littoral drift along the coast is calculated and presented in dimensionless diagrams for coasts with constant slope. The paper further analyzes the transverse distribution of the longshore sediment transport on a coast with bars. The last case is compared with field measurements.

INTRODUCTION

Sediment transport in near-shore areas is a complex three-dimensional phenomenon which often is split up into two parts, the on-off shore transport and the longshore transport. These two processes cannot be considered independently: for instance, the on-off shore sediment transport creates the bars on coasts where the change in water level due to tides only is moderate. Bars are created by onshore movement outside the breaker zone and offshore movement inside the breaker zone, see e.g. Ref. 6. These bars modify the longshore sediment transport distribution across the coast profile, as discussed later in this paper.

The information about on-offshore sediment transport is today very scarce and most research is correlated to the circulation of water under broken waves, see e.g. Ref. 6. Much more research has been done on the longshore sediment transport, where the transport mechanism has been known for several decades. On a coast without any external driven current, the sediment is transported by the longshore current generated in the surf zone due to a decrease in the radiation stresses (20). The sediment is picked up from the bottom due to the orbital wave motion which creates near-bed velocities normally much stronger than the nearbed longshore current velocities.

A first approach to quantify the above mechanism is the well-known CERC-formula (26), which simply relates the longshore sediment transport I_l in terms of the submerged weight to the "longshore energy flux factor" P_{ls} by

$$I_l = KP_{ls} \quad \ldots\ldots (1)$$

By this method, important parameters like grain sizes and the morphology of the coast (bars, slopes) are not taken into account.

A more theoretical approach has been carried out by Bijker (5), who calculated the sediment transport in several steps. First, he calculated

[1]Hydr. Engr., Danish Hydraulic Institute, Agern Alle 5 DK-2970 Hørsholm, Denmark.

[2]Assoc. Prof., Inst. of Hydrodynamics and Hydr. Engrg. (ISVA), Tech. Univ., Denmark, DK-2800 Lyngby, Denmark.

[3]ISVA. (Present address: Danish Hydraulic Institute).

Note.—Discussion open until October 1, 1986. To extend the closing date one month, a written request must be filed with the ASCE Manager of Journals. The manuscript for this paper was submitted for review and possible publication on May 2, 1985. This paper is part of the ***Journal of Waterway, Port, Coastal and Ocean Engineering***, Vol. 112, No. 3, May, 1986. ©ASCE, ISSN 0733-950X/86/0003-0351/$01.00. Paper No. 20595.

the longshore current induced by the incoming waves. Further on he calculated the variation in wave height perpendicular to the coast, taking into account the breaking of waves. Finally, from this combined wave-current motion he calculated the resulting sediment transport from a sediment transport formula.

The purpose of the present work is to introduce recently developed models for the vertical distribution of suspended sediment in combined wave-current motion in non-breaking waves (14) as well as in broken waves (9), the latter being an extension of Ref. 14. These models are combined with a detailed description of the change in wave height in the surf zone and in the longshore current distribution.

Hydrodynamic Description

The hydrodynamic description can be split up into two parts: (1) A macro scale description giving the gross-behavior of waves (refraction, shoaling, breaking) and current (longshore current distribution); and (2) a detailed description of the flow in a vertical in order to describe the vertical distribution of suspended sediment and the flow-resistance in combined wave-current motion.

Of course items (1) and (2) are interdependent. For instance the longshore current distribution is a function of the friction factor f in combined wave-current motion where f is evaluated under item (2).

In the following, the macro scale description is briefly outlined first. Later on we revert to the detailed flow description.

Variation in Wave Height

In the following, we consider a long straight shore line with parallel bottom contours. From deep water, the waves are refracted and shoaled

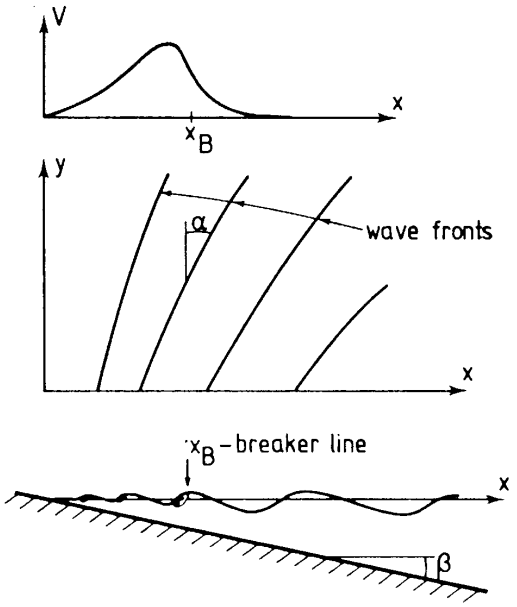

FIG. 1.—Definition of Longshore Current Profile, Wave Crests and Coastal Profile

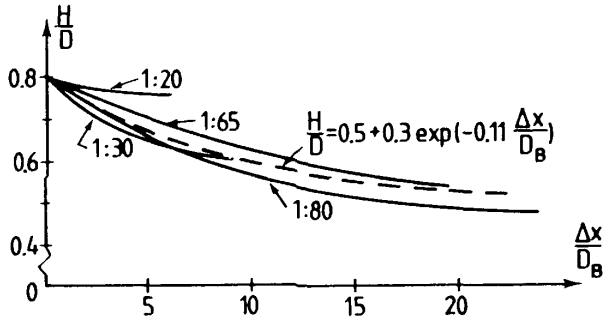

FIG. 2.—Variation in Wave Height after Breaking on Sloping Bottom. Measurements from Horikawa and Kuo (16)

until the breaking point, applying the usual refraction and shoaling theory for linear waves and assuming no energy dissipation. The waves are assumed to break where the wave height becomes equal 0.8 times the water depth, which is a reasonable approximation for small bed slopes. After breaking, the wave height decreases over a certain distance approaching a kind of equilibrium state, where the local wave height H is very close to half the local water depth (16,24). The transition from breaking to broken state can be approximated by the following expression

$$\frac{H}{D} = \gamma = 0.5 + 0.3 \exp\left(-0.11 \frac{\Delta x}{D_B}\right) \quad \ldots\ldots (2)$$

in which Δx = the distance from the breaking point, D = the water depth referring to mean water level, and D_B = the water depth at the breaking point. Eq. 2 is an analytical approach to the experiments described in Ref. 16, shown in Fig. 2. It is seen that Eq. 2 is a valid approximation for moderate bed slopes (less than about 1:30). Eq. 2 is originally proposed by Andersen and Fredsøe (1).

Longshore Current Distribution

The longshore current driven by the radiation stresses associated with the waves as described by Longuet-Higgins (20) is assumed to be the only current involved in the present study. The important component of the radiation stress tensor in relation to generation of longshore current is the "shear" component S_{xy}, given by

$$S_{xy} = F_m \cos(\alpha) \sin(\alpha) \quad \ldots\ldots (3)$$

in which α = the angle between the wave fronts and the coastline, Fig. 1, and F_m = the momentum flux in the direction of the wave propagation. Longuet-Higgins (20) showed that S_{xy} is constant in refracting waves as long as no energy is dissipated from the waves, i.e. no breaking occurs. When the waves are breaking, S_{xy} decreases towards the shoreline, giving a driving force: $\partial(S_{xy})/\partial x$.

The littoral current can then be found from the equation expressing

equilibrium between the following forces: (1) Radiation stress, gradient of S_{xy}; (2) flow resistance; and (3) transfer of momentum due to velocity gradients in the x-direction, x being the coordinate perpendicular to the coast.

The equation reads:

$$\frac{\partial(S_{xy})}{\partial x} = \tau_b - \frac{\partial}{\partial x}\left(\rho E D \frac{\partial V}{\partial x}\right) \quad \text{(4)}$$

in which τ_b = the bed shear stress from the current, y = the longshore coordinate, E = the momentum exchange coefficient and V = the current velocity.

The variation in S_{xy} across the surf zone is calculated from the expressions for the wave characteristics given in the section above using the linear wave theory.

To be correct, the shore normal momentum equation should also be included in the flow description in order to calculate set-down and set-up. In the present analysis, this is for reasons of simplicity not taken into account, whereby the longshore current is slightly underestimated very close to the shoreline, where the set-up is largest. However, the maximum sediment transport takes place close to the breaker line, so the above mentioned effect is rather small.

Flow Resistance.—The mean bed shear stress τ_b must be described for the combined three-dimensional wave-current motion, because the flow resistance is increased drastically when waves are superposed the current.

In the present paper, the flow resistance is calculated from Ref. 13, which describes the wave-current flow in arbitrary three-dimensional combinations.

The friction factor will be different for the wave and the current motion due to the large difference between the thicknesses of the wave boundary layer and the current boundary layer. The nonlinear (almost quadratic) relation between the mean bed shear stress and the current velocity gives a weaker relation between the slope and the current velocity than the linear resistance applied by Longuet-Higgins (20): a change in the beach slope of a factor 10 only changes the longshore current strength about a factor 2, as seen from the numerical example with the present model in Fig. 3.

The height of the breaking or broken waves is limited by the depth, γD. γ is a function of the distance from the breaking point (Eq. 2). If the water depth increases towards the coast, as it is the case on a barred coast, the limiting depth is taken as the depth at the crest of the bar. In this case the waves are re-established as non-breaking when the wave height is equal to half the depth over the bar. This model has been shown by Tucker, Carr and Pitt (25) to be in agreement with field measurements.

Momentum Transfer.—The exchange of momentum is described by use of an "eddy viscosity type" of exchange coefficient. Several mechanisms are active in the momentum transfer, such as the turbulent fluctuations in the breaker zone and circulation currents. The exchange coefficient is less important than the bed shear stress, as its effects are more

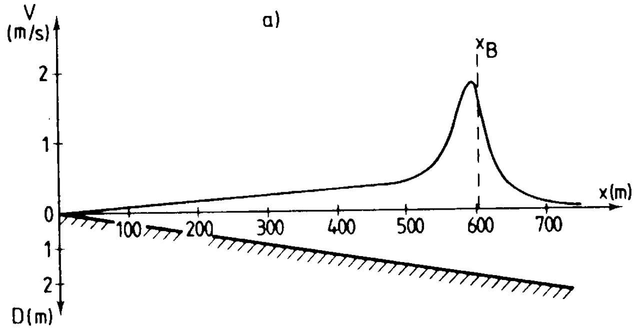

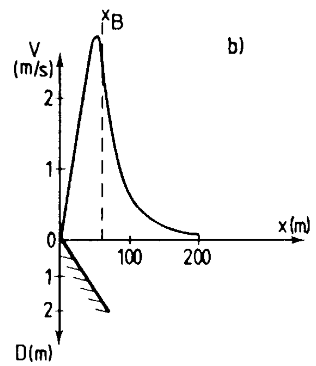

FIG. 3.—Examples of Longshore Current Profiles for Different Bed Slopes. Wave Characteristics: H_0 = 1.5 m, T = 6.2 s, α_0 = 45°. Bed roughness, k = 1.25 mm: (*a*) Bed slope, β = 1:333; (*b*) Bed slope, β = 1:33

to change the distribution of the velocities across the profile than to change the magnitude of the larger velocities close to the breaker line. In the present formulation the expression for E derived by Jonsson, Skovgaard and Jacobsen, Ref. 17,

$$E = \frac{4a^2}{T} \cos^2 \alpha \quad (5)$$

in which a = the near bed amplitude of the wave orbital motion and T = the wave period.

As shown in Ref. 17, large variations can be allowed in the momentum transfer coefficient E with only moderate changes in the longshore current as a result.

Numerical Solution.—Eq. 4 is solved numerically by a finite difference method with the boundary conditions $V = 0$ at the shore and $V \rightarrow 0$ for $x \rightarrow \infty$.

An example of a solution for a plane coast with constant slope has already been shown in Fig. 3. Fig. 4 shows how the longshore current is distributed across the coastal profile when bars are present. The profile is taken as the measured one at the Danish North Sea Coast (7). In Fig. 4(*a*) the incoming waves are assumed to be so large that they break at the outer bar. Hereby, a change in S_{xy} occurs at the outer bar until the water depth again becomes sufficiently high, and the waves are re-

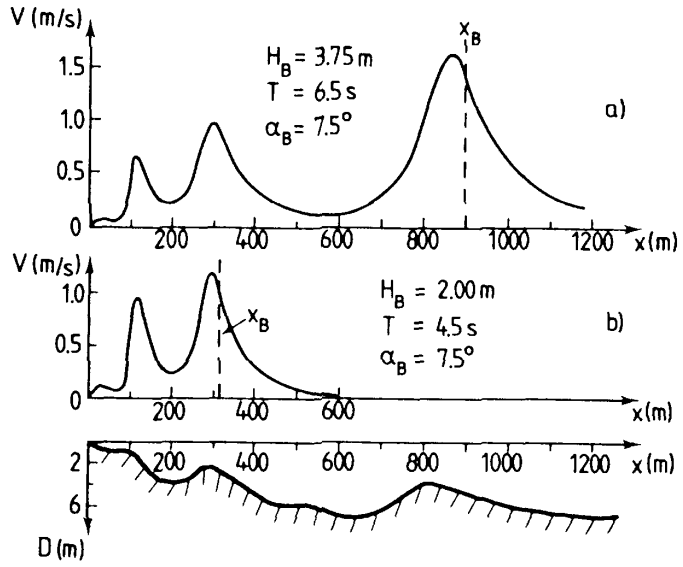

FIG. 4.—Calculated Longshore Current Profiles on Coast with Three Bars. Profile is Taken from (7). Wave Conditions Are Given at Outer Breaking Point: (*a*) Breaking on All Bars; (*b*) Breaking at Two Inner Bars

established at a smaller wave height, after which S_{xy} becomes constant until breaking takes place on bar number two. This means that the longshore current will be concentrated along the bars, as illustrated in Fig. 4(*a*). In case of smaller incoming waves, wave-breaking may not take place at the outer bar, which means that no longshore current will be generated at this bar at smaller wave activity, see Fig. 4(*b*).

Hydrodynamic Description of Turbulence.—In the case of non-breaking waves and no resulting current, the turbulence is restricted to a thin boundary layer just above the sea bed. Several methods are available to calculate this boundary layer, for instance Bakker and van Doorn (3), Grant and Madsen (15) and Fredsøe (13).

In the case of the presence of a current beside the waves, the turbulence is not only restricted to the thin wave boundary layer, but is extended to cover the entire flow depth.

All the three above mentioned models (Refs. 3, 13 and 15) are able to include a resulting current in their flow description in the case where the current is parallel to the direction of wave propagation. Further on, the models by Grant and Madsen (15) and by Fredsøe (13) are able to describe the general three-dimensional case, where the current forms an arbitrary angle with the direction of wave propagation. This is important in description of longshore sediment transport, because the current forms angles up to 90° with the direction of wave propagation in the surf zone.

In breaking and broken waves, turbulent kinetic energy is furthermore produced by the roller in the surface. Deigaard et al. (9) calculated the increase in the turbulent kinetic energy over the entire flow depth formed by the production of turbulent energy in a spilling breaker. The production was assumed to be equal to that of a hydraulic jump, and the

diffusion and dissipation of energy were calculated by a first order turbulence model.

Sediment Description.—With known properties of turbulence—for instance represented by an eddy viscosity ϵ—the distribution of suspended sediment is found from the diffusion equation

$$\frac{\partial c}{\partial t} = w\frac{\partial c}{\partial z} + \frac{\partial}{\partial z}\left(\epsilon_s \frac{\partial c}{\partial z}\right) \quad \ldots\ldots (6)$$

in which c = instantaneous concentration by volume; t = time; w = fall velocity of suspended sediment; z = the vertical coordinate; and ϵ_s = the instantaneous turbulent exchange factor for suspended sediment. ϵ_s is normally taken equal to the eddy viscosity for the flow. In the present model this eddy viscosity is in the case of non-breaking waves evaluated as outlined by Fredsøe et al. (14), applying the flow description by Fredsøe (13). In breaking waves, the description by Deigaard et al. (9) has been applied.

In order to solve Eq. 6, two boundary conditions are needed. One is the requirement of no flux of sediment in the surface or

$$wc + \epsilon_s \frac{\partial c}{\partial z} = 0 \quad \text{at} \quad z = D \quad \ldots\ldots (7)$$

The other boundary condition is correlated to the bed concentration c_b. In the present investigation the bed is assumed plane, so the bed roughness k is scaled to the mean grain diameter d. For the present we have taken $k = 2.5\,d$. This result is known to be valid in uni-directional flow in the plane bed regime at large shear stresses, (12). As pointed out by Dingler and Inman (10), wave generated ripples disappear at large near-bottom flow velocities. Nielsen (22) analyzed the ripple data and found that the disappearance of the ripples took place for the Shields' parameter θ being in the interval $0.8 < \theta < 1.0$. Shields' parameter θ is the dimensionless bed shear stress defined by

$$\theta = \frac{\tau_{b,\max}}{\rho(s-1)gd} \quad \ldots\ldots (8)$$

in which $\tau_{b,\max}$ = the maximum bed shear stress during a wave-cycle, ρ = fluid density, s = relative density of sand (~2.65), g = acceleration of gravity, and d = mean grain diameter.

By inspection of typical data on wave heights and wave periods during storm situations one finds that typical values of θ are in the range of $1 < \theta < 10$–20. This estimate is of course rough, but indicates that most sediment transport in coastal areas takes place while the bed is plane, i.e. no ripples on the bed.

Keeping this in mind, the bed concentration c_b of suspended sediment can be found by the method suggested by Engelund and Fredsøe (11), who applied the dynamic principles of Bagnold (2) to predict the bed concentration of suspended sediment as function of the instantaneous Shields' parameter θ.

Fig. 5 demonstrates through a numerical example how the models in Refs. 9 and 14 work: in case of non-breaking waves the suspended sed-

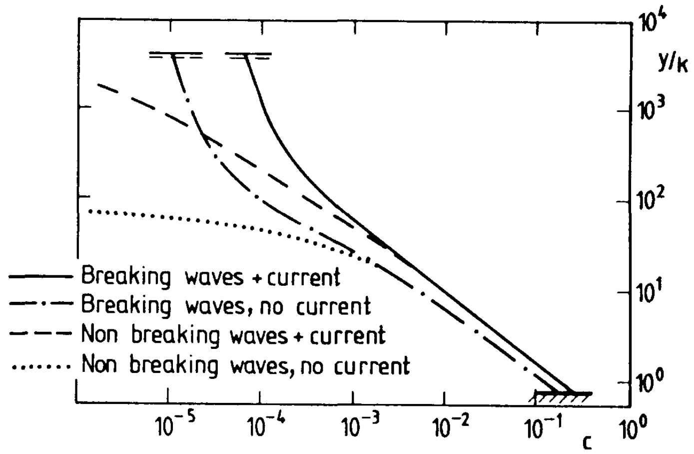

FIG. 5.—Suspended Sediment Concentrations Profiles in Breaking and Non-Breaking Waves. Example Is Based on: D = 2 m, H = 1 m, T = 6 sec, d = 0.2 mm, and V = 1 m/s

iment is restricted to the thin turbulent wave boundary layer of thickness some hundred times the bed roughness. If the waves are breaking, the near bed concentration remains nearly the same for a given wave height and wave period. However, farther away from the bed the concentration of suspended sediment increases tremendously due to increase in turbulence intensity. Further on, Fig. 5 demonstrates that the presence of a resulting current also increases the concentration of suspended sediment farther away from the bed.

With known vertical distribution of suspended sediment the longshore transport of sediment per unit width perpendicular to the coast is found by

$$q_s = \frac{1}{T}\int_0^T dt \left[\int_0^D cU\,dz\right] \quad (9)$$

U = the instantaneous velocity of the combined wave current motion. The bed shear stress and the depth averaged mean current velocity V are both obtained by an iterative solution of Eq. 4, applying the flow-resistance model by Fredsøe (13). Hereby, the vertical and temporal variation of U is obtained too. The application of Ref. 13 is of course an approximation in the breaker zone where the turbulence generated by the wave breaking will modify the current velocity profile slightly, as seen from the following considerations: the longshore current is driven by the shear component of the radiation stress, whereby the vertical shear stress distribution differs from the normal linear distribution in open channel flow. As an extreme, the driving force can be assumed to be concentrated near the surface (in the roller) whereby the vertical shear stress distribution becomes rectangular. Fig. 6 illustrated through a numerical example the importance of this effect: the dotted line shows the calculated time averaged velocity $\bar{U}$ based on a linear distribution of shear stress, while the dashed shows $\bar{U}$ based on a rectangular shear stress

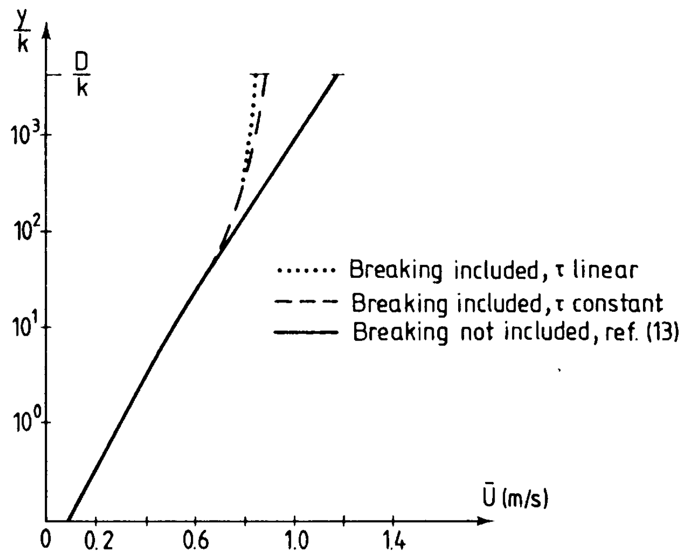

FIG. 6.—Example of Effect of Surface Roller on Mean Current Velocity in Surf Zone for H = 1 m, T = 6 sec, and D = 2 m

distribution. Both profiles include the turbulence generated by wave-breaking applying the eddy viscosity ϵ as calculated in Ref. 9. The deviation between the two calculated profiles is very small. The fully drawn line in Fig. 6 shows the velocity profile obtained by the theory of Ref. 13, neglecting the wave-breaking. It is seen that the effect of surface generated turbulence is most significant far from the bed where the sediment concentrations are smallest. The effect on the suspended load transport is in the present example 12%, which justifies the application of the theory developed in Ref. 13 as an approximation even in the surf zone.

Besides the suspended sediment, the transport of bed load is incorporated in the model. However, at θ-values larger than 1, the bed load transport is negligible compared to the transport of suspended sediment transport.

The total longshore sediment transport Q_S in grain volume is now found by integration perpendicular to the coast to be

$$Q_S = \int_0^\infty q_s \, dx \qquad (10)$$

Comparison with Field Data

Comparison of the present theory with laboratory experiments has not been carried out. In a laboratory, the bed will normally be covered by wave-ripples, which together with laminar effects in the wave boundary layer may cause large scale errors in the evaluation of the strength of longshore current and in the vertical distribution of suspended sediment. For this reason, we have chosen to compare with a field study instead.

The amount of field data which is required for comparison with a detailed littoral drift model as the present is very comprehensive. Such ideal data should comprise: (1) Wave characteristics; (2) sediment characteristics in the coastal zone; (3) current velocities in the surf zone; (4) bathymetry; and (5) the distribution of the sediment transport rate in the coastal profile. Only very few sets of field data are available which satisfy at least some of the requirements above. Further, in most of the reported field measurements comparison has been made with the CERC-formula, leading to a reduction of the reported data with focus on the "longshore energy flux factor," which is the parameter used in the CERC-formula.

One of the most comprehensive field investigations of longshore sediment transport has recently been reported by the Danish Hydraulic Institute (7,21). Here the complete natural backfilling of a 1,600 m long trench, dredged through a three-bar coastal profile at a straight reach of the Danish West Coast has been monitored. A typical profile is depicted in Fig. 4. The soundings of the trench were made six times during the period of backfilling, and recordings were made of wind, waves and current velocities at 12 m water depth. Unfortunately, no flow measurements could be performed in the surf zone.

It has been chosen to compare results of the theoretical model with the recorded backfilling between March 22nd and April 15th, 1982. This period has been chosen because a significant backfilling occurred in a relatively short time, and this backfilling can be related to a single storm period (April 7th–10th) with significant wave height up to 4.75 m.

At the time of the storm, the trench was only dredged across the outer bar ($x > 400$ m). The distribution of the backfilling is shown in Fig. 7.

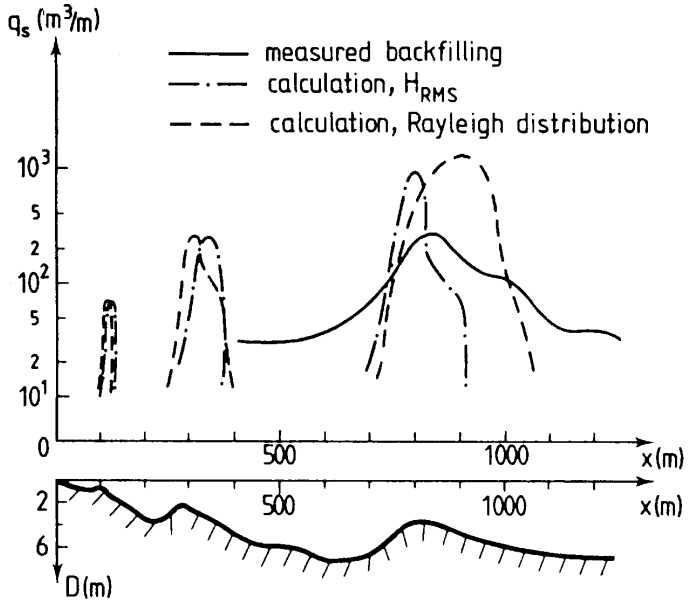

FIG. 7.—Distribution Across Coast Profile of Backfilling of Trench and Calculated Longshore Sediment Transport. The Measured Data Are from (7)

The total backfilling is approx. 90,000 m^3 (solid) grain volume.

The width of the trench was 90 m and the depth 10 m, which justify that almost all sediment transported longshore was trapped in the trench.

Storm waves are of course irregular and three-dimensional, and it is not trivial to find the input conditions to the mathematical model which corresponds to the field conditions. Two approaches have been applied:

1. The root mean square, H_{rms}, of the breaking heights has been applied. It has been shown by Rasmussen and Fredsøe (23) that calculations using H_{rms} gave the best agreement with laboratory experiments with sediment transport under irregular waves and a current.
2. It has been assumed that the wave heights follow the Rayleigh distribution, and the sediment transport, Q_s, has been calculated accordingly:

$$Q_s = \int_0^\infty f_r(H) Q_s(H) dH \quad \text{(11)}$$

in which f_r = the probability density function of the Rayleigh distribution. The correlation between wave period and wave height is based on the scatter diagram in Ref. 7. With this approach it has implicitly been assumed that the longshore current always corresponds to the instantaneous wave, i.e. that a single high wave will coincide with a high longshore current velocity. Due to the nonlinear sediment transport relations this could be expected to lead to an over-prediction of the sediment transport.

For both methods the calculation has been performed for the combinations of significant wave heights and wave directions given by Mangor et al. (21) for the period of backfilling. For all situations with waves breaking at the outer bar a south-going sediment transport is predicted, and the backfilling is compared with the total calculated transport.

The total amounts of calculated littoral drift (on the outer bar only) are given in Table 1.

The calculated distributions of sediment transport across the coastal profile are shown in Fig. 7. It is seen that the theory predicts the littoral drift to be concentrated on the bars. This is partly due to the concentration of the longshore current along the bars, cf. Fig. 4, partly due to the smaller water depth above the bars. The latter results in larger near-

TABLE 1.—Comparison between Calculated and Measured Sediment Transport. Mean Grain Diameter is 0.20 mm

Description (1)	Total amount (m^3) (2)	Ratio between calculation and measurement (3)
Measured backfilling	90.000	—
Calculated on basis of H_{rms}	50.000	0.6
Calculated on basis of Rayleigh distribution	205.000	2.3

bed wave induced flow velocities, and therefore larger concentrations of suspended sediment. Finally, the sediment transport capacity is largest in breaking waves, the breaking being concentrated around the bars.

It appears that the calculated distribution is more peaked than the measured backfilling, especially the one based on H_{rms}. This may be partly attributed to the current model which is based on regular waves. It has been shown by Battjes (4) that the longshore current profile will be more smooth for irregular waves, because the wave breaking will be distributed over a wider zone rather than occurring at a breaker line.

Apart from the irregularity of the waves there are some uncertainties involved in the evaluation of the measurements. The most severe uncertainty is probably that the actual coastal profile during the storm is unknown. The sounded profiles after a storm may well be formed by the less severe conditions at the last part of the storm. A small variation in the height or shape of the bar may affect the amount and distribution of the sediment transport. Another unknown factor is the effect of the trench itself on the wave and current pattern.

Diagrams and Formulas of Applications

This section presents diagrams and formulas which can be applied to quantify the littoral drift along a straight coast with constant slope. As the littoral drift is concentrated in a rather narrow zone around the breaking point, the findings may be applicable for a more complicated bed profile by putting the slope equal to the slope around the point of breaking.

As seen from Fig. 3, the longshore current velocity increases slightly with increasing bed slope. On the other hand, the width of the transport zone decreases. These two items result totally in an increase in the total sediment transport, Q_s, which is found to be approximately proportional to $\sqrt{\beta}$. This can be seen from Fig. 8, which shows the variation of the dimensionless total sediment transport, Φ, with β for four different combinations of wave height and sediment size. Here Φ is defined by

$$\Phi = \frac{Q_s}{H_0\sqrt{\beta}\sqrt{(s-1)gd^3}} \quad \ldots\ldots (12)$$

in which H_0 = the deep waterwave height. Φ will be a function of the following dimensionless parameters: bed slope β, deep water wave height H_0/d, deep water wave steepness H_0/L_0, where L_0 = deep water wave length, the angle α_0 between coast and deep water wave crest, and finally sediment settling velocity w^*, defined by

$$w^* = \frac{w}{\sqrt{gd}} \quad \ldots\ldots (13)$$

in which w = fall velocity of sediment.

Fig. 8 shows that Φ is almost constant for a variation in β over one decade. In the following the influence of the bed slope on the transport will be taken into account through the definition of Φ.

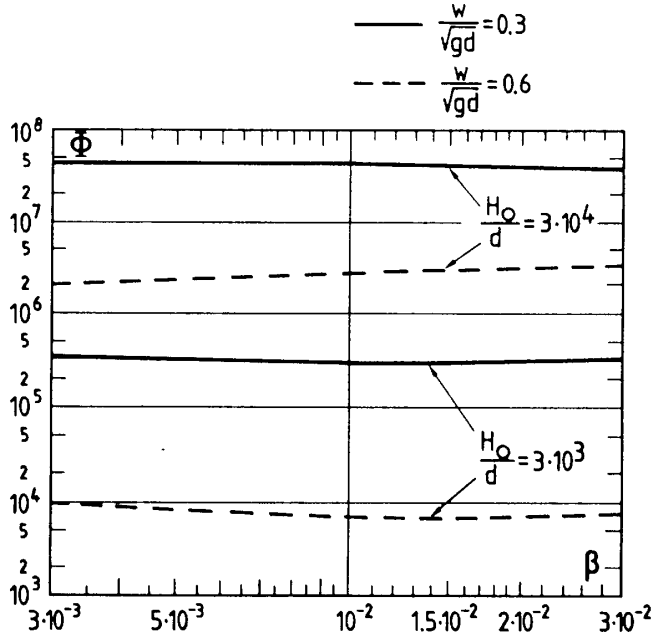

FIG. 8.—Variation in Φ with Bed Slope β, $\alpha_0 = 45°$

The variation in different parameters with the deep water wave direction is shown in Fig. 9 for a single combination of wave height, wave steepness, and settling velocity. Besides the sediment transport, the variation in the maximum current velocity and in the "longshore energy flux factor" at breaker line, P_{ls}, is shown. The latter indicates the variation in littoral drift according to the CERC-formula (26).

The variation in Q_s with deep water wave angle depicted in Fig. 9(*a*) is typical for a large range of H_0/d, w^* and H_0/L_0. A curve fitted to this variation is

$$\frac{Q_s}{Q_{s,\max}} = \left(\sin\left\{2\alpha_0\left[1 - 0.4\,\frac{\alpha_0}{90°}\left(1 - \frac{\alpha_0}{90°}\right)\right]\right\}\right)^{5/2} \quad \ldots\ldots\ldots\ldots\ldots\ldots \quad (14)$$

which can be used as an approximation for the variation of the sediment transport with the wave direction.

The sediment transport at $\alpha_0 = 45°$, Φ_0, is shown in Fig. 10 as a function of H_0/d, w^* and H_0/L_0. As described earlier, the model is only valid for a flat bed without ripples, which corresponds to a minimum wave height, H_0, of approximately 2,000 d.

The curves shown in Fig. 10 can for $H_0/d < 3 \times 10^4$ be approximated by the following expression with an accuracy within 10%:

$$\Phi_0 = \left(\frac{\frac{H_0}{d}}{10^4}\right)^P 1.8 \times 10^7 \left(\frac{H_0}{L_0}\right)^{0.42} \exp\left\{\left(-8.9 + 65\,\frac{H_0}{L_0}\right)(w^* - 0.3) + \left[4.0 - 65\left(\frac{H_0}{L_0}\right)\right](w^* - 0.3)^2\right\} \quad \ldots\ldots\ldots\ldots\ldots\ldots\ldots\ldots \quad (15)$$

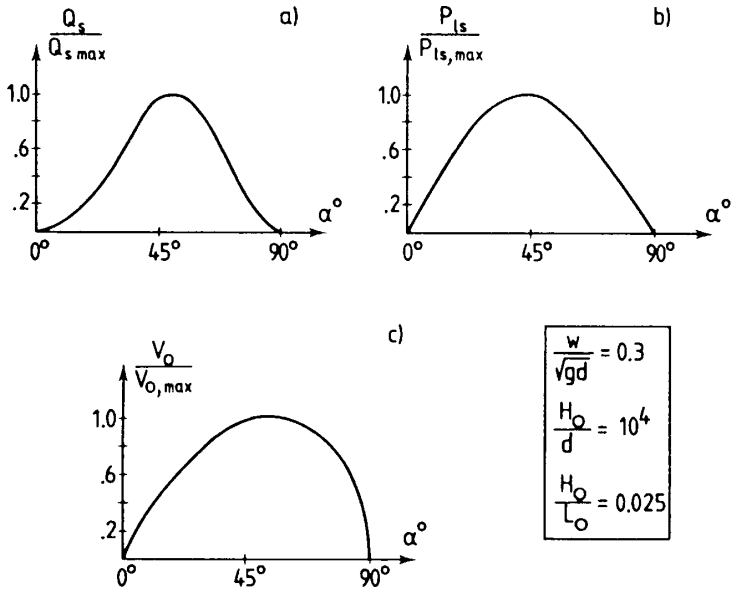

FIG. 9.—(*a*) Variation in Littoral Drift; (*b*) "Longshore Energy Flux Factor"; (*c*) Maximum Littoral Current Velocity with α_0

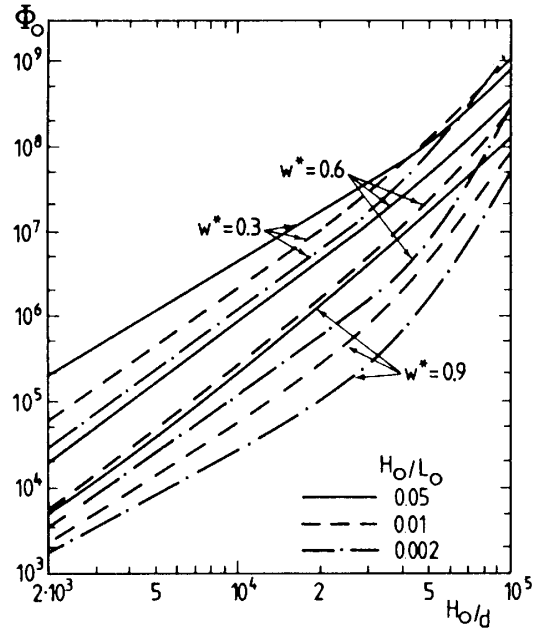

FIG. 10.—Variation of Longshore Transport with Grain Size, Wave Steepness and Wave Height, $\alpha_0 = 45°$

in which

$$P = 2.79 + 0.069 \ln\left(\frac{H_0}{L_0}\right) - 1.67\left[1.46 + 0.187 \ln\left(\frac{H_0}{L_0}\right) - w^*\right]^2 \quad \ldots\ldots (16)$$

A less elaborate expression than Eqs. 15 and 16 is

$$\Phi_0 = 0.1 \left(\frac{H_0}{d}\right)^{2.3} \left(\frac{H_0}{L_0}\right)^{1/2} \exp(-6.1\, w^*) \quad \ldots\ldots\ldots\ldots\ldots\ldots\ldots\ldots\ldots\ldots \quad (17)$$

which produces the curves in Fig. 10 within 50%.

These expressions can be combined with Eq. 14 to obtain estimates for other wave directions than $\alpha_0 = 45°$.

As mentioned in the introduction, the CERC-formula is the most commonly used littoral drift formula. This is partly because of its simplicity, but also because it is supported by a lot of field measurements, although with large scatter. It is therefore relevant to compare the present model to the CERC-formula.

The variation with the wave direction has been illustrated in Fig. 9, where it is noticed that the transport according to this model is relatively

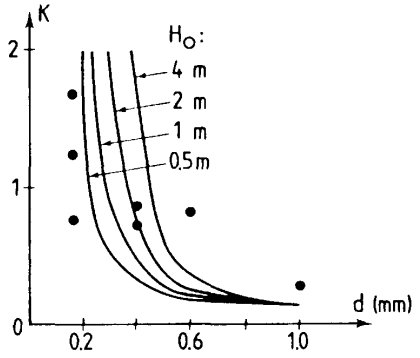

FIG. 11.—Variation in K-Factor with Grain Size. Theoretical Prediction Is Based on $H_0/L_0 = 0.025$, $\beta = 0.01$, and $\alpha_0 = 45°$. The Measured Values (Filled Circles) Are from Ref. 8

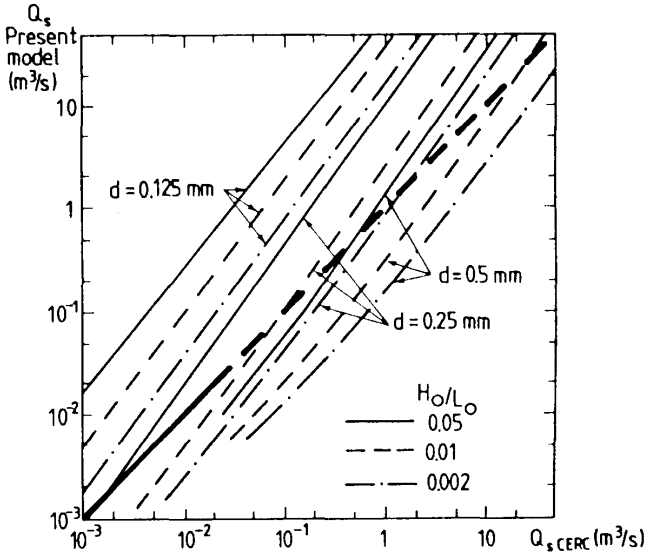

FIG. 12.—Comparison Between Present Model and CERC-Formula for $\alpha_0 = 45°$

smaller for small and large values of α_0 than predicted by the CERC-formula.

Another important parameter in the CERC-formula is the wave height, and the littoral drift is approximately proportional to the wave height in a power 2.5. The dependency of the wave height is stronger in this model, where the power on the wave height is about 3–3.5.

The grain size is a very important parameter in the present model, as in all sediment transport models. No sediment characteristics enter the CERC-formula, which may be because of a small variation in the grain size between the different sites where data have been obtained for the CERC-formula.

Komar and Inman (19) suggest a value of $K = 0.77$ in Eq. 1. Based on measurements, Dean, Berek, Gable and Seymour (8) have proposed a relation between the grain size of the beach sediment and the factor K. An example of the variation obtained by the present model is shown in Fig. 11, together with the points forming the basis for Dean's relation. The tendency is the same, namely increasing transport with decreasing grain size.

A comparison between the present mathematical model and the CERC-formula is shown in Fig. 12 for $\alpha_0 = 45°$ and $\beta = 0.01$. The line of perfect agreement is shown as a fully drawn line in the region where the CERC-formula is supported by empirical data. The two models can be seen to predict littoral drifts of the same order of magnitude for a grain size of about 0.2 mm. Changes in α_0 or β would result in a displacement of the curves in Fig. 12, but not a change in their shape.

Conclusion

A mathematical model for littoral drift is presented which includes a detailed hydrodynamic as well as a detailed sediment behavior description.

The paper first describes the littoral drift along a bar coast. The model predicts that the littoral drift is concentrated on the bars. This is partly due to smaller local water depth, partly due to large longshore current on the bars, and finally due to larger transport capacity under broken waves.

This model has been compared with a field study at the Danish North Sea coast, and the agreement has been found to be satisfactory, taking into account the complexity of the treatment of an irregular wave climate.

In case of a coast with constant slope, dimensionless diagrams have been worked out for calculation of the littoral drift.

The present theory suggests that the littoral drift not only is a function of the "longshore energy flux factor," but also of the slope of the coast and the sediment properties: the littoral drift increases nearly by the square root of the slope, and increases very much with decreasing grain size.

For grain sizes around 0.2 mm, which is very common on beaches, the present theory does not deviate much from the CERC-formula. The present theory further on predicts the transverse distribution of the longshore sediment transport on the coastal profile.

Acknowledgment

One of the writers (Rolf Deigaard) is supported by the Danish Technical Research Council (STVF).

Appendix I.—References

1. Andersen, O. H., and Fredsøe, J., "Transport of suspended sediment along the coast," Institute of Hydrodynamics and Hydraulic Engineering, Technical Univ. of Denmark, Prog. Rep. 59, 1983, pp. 33–46.
2. Bagnold, R. A., "Experiments on a gravity-free dispersion of large solid spheres in a Newtonian fluid under shear," Proceeding Royal Society, London (A) 225, 49, 1954.
3. Bakker, W. T., and van Doorn, T., "Near-bottom velocities in wave with current," Coastal Engineering Conference, 1978, pp. 1394–1413.
4. Battjes, J. A., "Computation of set-up. Longshore currents, run-up and over topping due to wind-generated waves," Delft Technishe Hogeschool, 1974, 244 pp.
5. Bijker, E. A., "Longshore Transport Computations," *Journal of the Waterways, Harbors and Coastal Engineering Division*, ASCE, Vol. 97, No. WW4, Nov., 1971, pp. 687–701.
6. Dally, W. R., and Dean, R. G., "Suspended sediment transport and beach profile evolution," *Journal of Waterway Port Coastal and Ocean Engineering*, ASCE, Vol. 110, No. 1, 1984.
7. Danish Hydraulic Institute, "North Sea shore approach, monitoring of sedimentation in a dredged trench," Research report, Copenhagen, 1984.
8. Dean, R. G., Berek, E. P., Gable, C. G., and Seymour, J., "Longshore transport determined by an efficient trap," Coastal Engr. Conf., 1982, pp. 954–968.
9. Deigaard, R., Fredsøe, J., and Hedegaard, I. B., "Suspended sediment in the surf zone," Vol. 112, No. 1, 1986, pp. 115–128.
10. Dingler, J. R., and Inman, D. L., "Wave-formed ripples in nearshore sands," 15, Coastal Engineering Conference, 1976, pp. 2109–2126.
11. Engelund, F., and Fredsøe, J., "A sediment transport model for straight alluvial channels," *Nordic Hydrology*, 7, 1976, pp. 293–306.
12. Engelund, F., and Hansen, E., "A monograph on sediment transport in alluvial streams," Technical Press, Copenhagen, Denmark, 1972.
13. Fredsøe, J., "The turbulent boundary layer in combined wave-current," *Journal of Hydraulic Engineering*, ASCE, Vol. 110, No. HY8, 1984, pp. 1103–1120.
14. Fredsøe, J., Andersen, O. H., and Silberg, S., "Distribution of suspended sediment in large waves," *Journal of the Waterway Port Coastal and Ocean Engineering*, ASCE, Vol. 111, No. 6, 1985, pp. 1041–1059.
15. Grant, W. D., and Madsen, O. S., "Combined wave and current interaction with a rough bottom," *Journal of Geophysical Research*, Vol. 84, 1979, pp. 1797–1808.
16. Horikawa, K., and Kuo, C.-T., "A study on wave transformation inside surf zone," Coastal Engineering Conference, Vol. 1, 1966, pp. 217–233.
17. Jonsson, I. G., Skovgaard, O., and Jacobsen, T. S., "Computation of longshore currents," Proc. Coastal Engineering Conference, 1974, pp. 699–714.
18. Komar, P. D., *Beach processes and sedimentation*, Prentice Hall, Inc., Englewood Cliffs, N.J., 1976.
19. Komar, P. D., and Inman, D. L., "Longshore sand transport on beaches," *Journal of Geophysical Research*, Vol. 75, No. 30, 1970, pp. 5914–5927.
20. Longuet-Higgins, M. S., "Longshore currents generated by Obliquely Incident Sea Waves, 1 and 2," *Journal of Geophysical Research*, Vol. 75, 1970, pp. 6778–6801.
21. Mangor, K., Sørensen, T., and Navntoft, E., "Shore approach at the Danish North Sea Coast, monitoring of sedimentation in a dredged trench," Proc.

Coastal Engineering Conference. In print, 1984.
22. Nielsen, P., "Some basic concepts of wave sediment transport," Series Paper 10, Inst. of Hydrodyn. and Hydraulic Engineering, Techn. Univ. of Denmark, 1979.
23. Rasmussen, P., and Fredsøe, J., "Measurements of sediment transport in combined waves and current," Prog. Rep. 53, Inst. of Hydrodyn. and Hydraulic Engineering, Techn. Univ. of Denmark, 1981, pp. 27–30.
24. Stive, M. J. F., "Velocity and pressure field of spilling breakers," Delt Hydraulics Laboratory, No. 233, 1980.
25. Tucker, M. J., Carr, A. P., and Pitt, E. G., "The effect of an offshore bar in attenuating waves," Coastal Engineering, Vol. 7, No. 2, 1983, pp. 122–144.
26. U.S. Army, Coastal Engineering Research Center, *Shore Protection Manual*, third edition, 1977.

APPENDIX II.—NOTATION

The following symbols are used in this paper:

a = near bed amplitude of the wave orbital motion;
c = suspended sediment concentration;
c_b = bed concentration of suspended sediment;
D = water depth;
D_B = water depth at the breaking point;
d = grain diameter;
E = momentum exchange coefficient;
F_m = momentum flux in the direction of wave propagation;
f = friction factor;
f_r = probability density function of the Rayleigh distribution;
g = acceleration of gravity;
H = wave height;
H_{rms} = root-mean square of the wave heights;
H_0 = deep water wave height;
I = integral, defined in Eq. 5;
I_l = the longshore sediment transport rate, given as submerged weight;
K = coefficient in the CERC formula;
k = bed roughness;
L_0 = deep water wave length;
P_{ls} = "longshore energy flux factor";
P = power used in approximate formula for Φ_0;
Q_s = longshore sediment transport;
q_s = longshore sediment transport rate per unit width;
S_{xy} = shear component of the radiation stress tensor;
s = relative density of the sediment;
T = wave period;
t = time;
U = instantaneous flow;
$\bar{U}$ = time averaged current velocity;
V = longshore current velocity, depth averaged;
V_0 = maximum of V;
w = settling velocity of suspended sediment;
w^* = dimensionless settling velocity;

x = distance from the coast line;
y = vertical coordinate;
z = longshore coordinate;
α = angle between the wave fronts and the coast line;
α_0 = deep water wave angle;
β = coastal slope;
γ = ratio between H and D for breaking and broken waves;
Δx = distance from the breaking point, measured in the inshore direction;
ϵ = eddy viscosity;
ϵ_s = turbulent diffusion coefficient for suspended sediment;
θ = dimensionless bed shear stress;
ρ = density of water;
τ_b = bed shear stress from the current;
$\tau_{b,max}$ = maximum bed shear stress during a wave period;
Φ = dimensionless longshore sediment transport; and
Φ_0 = Φ for $\alpha_0 = 45°$.